Glycerol dialkyl glycerol tetraethers and the TEX_{86} index in sinking particles in the western North Pacific

Masanobu Yamamoto[1,*], Akifumi Shimamoto[2], Tatsuo Fukuhara[2], Yuichiro Tanaka[3], Joji Ishizaka[4]

[1]Faculty of Environmental Earth Science, Hokkaido University, Sapporo 060-0810, Japan.

[2]The General Environmental Technos Co., LTD., Osaka 541-0052, Japan.

[3]National Institute of Advanced Industrial Science and Technology, Tsukuba, Ibaraki 305-8567, Japan

[4]Hydrospheric Atmospheric Research Center, Nagoya University, Nagoya 464-8601, Japan

*Corresponding author; myama@ees.hokudai.ac.jp

Seasonal and depth variations in the flux of glycerol dialkyl glycerol tetraethers (GDGTs) and TEX_{86} (TEX_{86}^{H} and TEX_{86}^{L}) values in sinking particles were examined by conducting a 21-month time-series sediment trap experiment at a mooring station (WCT-2, 39°N, 147°E) in the mid-latitude NW Pacific. The aim of the study was to understand the sinking process of GDGTs in the water column and the preservation of the TEX_{86} signal in the water column and the sediment surface. In the shallow trap, the sinking flux of GDGT showed maxima from May 1998 to February 1999. The maximal

peaks of GDGT sinking flux corresponded to the peaks of the sinking fluxes of organic carbon, opal and lithogenic material. GDGT concentrations in the total fine fraction and the ratio of caldarchaeol to crenarchaeol at three different depths (~1300–4800 m) varied synchronously, implying rapid vertical transport of GDGTs to deeper water with a sinking velocity higher than 260 m d^{-1} below ~1300 m. The changes in TEX_{86}-based temperature were different from those in the contemporary SSTs. The TEX_{86}-based temperature was lower than the SST from May to December and corresponded to the temperature at the thermocline, whereas it was higher than the SST from December to May. The annual average sinking flux of the GDGTs decreased with increasing depth. The GDGT half-depth, the depth range over which half of the GDGT is lost, was calculated to be 3108–3349 m, implying that GDGTs were well preserved during sinking in the water column. The flux-weighted average TEX_{86}-based temperatures were constant with depth and roughly corresponded to mean annual SST. These findings support a previously proposed hypothesis that the GDGTs produced in surface waters are preferentially delivered to the deeper water column by grazing and repackaging in larger particles. The constant TEX_{86} at different depths indicates that TEX_{86} is not affected by degradation in the water column. The preservation efficiency of GDGTs was 1.0–1.3% at the water-sediment interface. Despite the significant degradation of the GDGTs, there was a small difference in TEX_{86} levels between sinking particles and the surface sediment.

Key words: TEX_{86}, glycerol dialkyl glycerol tetraether, sediment trap, Thaumarchaeota, North Pacific

48 **1. Introduction**

49 Glycerol dialkyl glycerol tetraethers (GDGTs) are ubiquitous in marine water and
50 sediments, and are thought to be derived mainly from marine Crenarchaeota Group I
51 (Sinninghe Damsté et al., 2002b), and marine Crenarchaeota Group I was recently
52 classified into a newly-defined archaeal phylum Thaumarchaeota (Brochier-Armanet et
53 al., 2008; Spang et al., 2010). The GDGTs biosynthesized by this group include
54 GDGT-0 (caldarchaeol)–GDGT-3, containing zero to three cyclopentane moieties, and
55 crenarchaeol, which has a cyclohexane moiety in addition to four cyclopentane moieties
56 (Schouten et al., 2000; Sinninghe Damsté et al., 2002b). Schouten et al. (2002)
57 proposed a new palaeotemperature index, TEX_{86}, based on the distribution of GDGTs
58 by way of an empirical correlation between TEX_{86} values in marine core top sediments
59 and sea surface temperatures (SSTs). Investigation of such a correlation has since been
60 developed using larger data sets (Kim et al., 2008; 2010). The application of TEX_{86} is
61 increasing in palaeoceanographic studies (e.g. Huguet et al., 2006b).

62 Multiple proxy approaches to the analysis of cores and surface sediments often show
63 inconsistent patterns when different proxy records are used (e.g., Huguet et al., 2006b,
64 Lee et al., 2008; Lopes dos Santos et al., 2010; Shintani et al., 2011). This phenomenon
65 has been generally attributed to differences in the season or depth that each proxy
66 reflects, physiological bias, or lateral advection. The TEX_{86} proxy is still under
67 development, and the production season and depth of GDGTs are still not clear. TEX_{86}
68 must be investigated further for better interpretation of proxy records.

69 Thaumarchaeota live throughout the water column (e.g., Murray et al., 1999; Karner
70 et al., 2001; Herndl et al., 2005; Baltar et al., 2007; Coolen et al., 2007; Agogué et al.,
71 2008; Beman et al., 2008; Verala et al., 2008). They occur in highest abundances in the

upper 100 m, but are also present in waters as deep as 5000 m (Karner et al., 2001; Herndl et al., 2005). The physiology of Thaumarchaeota in marine environments is not fully understood, although both heterotrophs (e.g., Ouverney and Furman, 2000; Agogué et al., 2008; Zhang et al., 2009) and chemoautotrophic nitrifiers (e.g., Könneck et al., 2005; Hallam et al., 2006; Wuchter et al., 2006a; Coolen et al., 2007; Beman et al., 2008; Park et al., 2010; Blainey et al., 2011; Pitcher et al., 2011) have been recognized. Agogué et al. (2008) suggested that Thaumarchaeota in subsurface waters (100–150 m) are mostly autotrophic, whereas they live heterotrophically in bathypelagic waters (>1000 m). In the South China Sea, the contribution of Thaumarchaeota to the total prokaryotic community was found to increase with depth and was higher in the upper mesopelagic water column inside than outside cold-core eddies, suggesting that the supply of refractory dissolved organic matter by upwelled water led to a more prominent abundance of Thaumarchaeota (Zhang et al., 2009).

Little is also known about the abundance of GDGTs in the water column. Sinninghe Damsté et al. (2002a) described maxima of crenarchaeol concentrations at 70 m and 500 m in the Arabian Sea. Wuchter et al. (2005) reported a high concentration of GDGTs in particulate organic matter (POM) in the deep-water column below 100 m. The abundance of GDGTs also varies seasonally. A high abundance was reported for winter in the North Sea (Wuchter et al., 2005; Herfort et al., 2006), suggesting that Thaumarchaeota thrive in winter because they do not need to compete with phytoplankton for NH_3. This hypothesis was recently supported by the observation that the abundance of intact GDGTs and Thaumarchaeota 16S rRNA genes and amoA genes showed a seasonal cycle with maxima in winter in the North Sea (Pitcher et al., 2011). Turich et al. (2007) reported the variability in GDGT composition in the water column

96 in different oceanographic settings and suggested that changes in archaeal ecology,
97 nutrient concentration and oceanographic conditions potentially affect TEX_{86}. Coolen et
98 al. (2007) described a maximum for crenarchaeol concentration in the sulfidic
99 chemocline in the water column of the Black Sea. In order for TEX_{86} to be a more
100 robust palaeotemperature proxy, a better understanding of the season and depth of
101 GDGT production is required.

102 It is critical to understand how surface water signals are propagated to deeper waters.
103 Wuchter et al. (2005) reported that the TEX_{86}-derived temperatures of POM at all
104 depths below 100 m correspond to SSTs. On the basis of this observation, they
105 concluded that the GDGTs produced in surface waters were preferentially delivered to
106 the deeper water column by grazing and repackaging in larger particles. Sediment-trap
107 studies conducted in the north-eastern Pacific Ocean and the Arabian Sea demonstrated
108 that the TEX_{86} values in sinking particles corresponded to SSTs, supporting the above
109 hypothesis (Wuchter et al., 2006b). In the Puget Sound, intact GDGTs are largely
110 present in the free-living particle size fraction (0.2 to 0.7 μm) and core GDGTs are
111 enriched in suspended (0.7 to 60 μm) and aggregate (>60 μm) size fractions, suggesting
112 that archaeal biomass quickly becomes attached or entrained in particles once the
113 archaea are dead or dying (Ingalls et al., 2012). This observation is consistent with the
114 hypothesis of Wuchter et al. (2006b). In contrast, variations in TEX_{86} values in sinking
115 particles were not coupled to SSTs or deep water temperatures in the Santa Barbara
116 Basin, which was attributed to a complex combination of the contributions of GDGTs
117 produced in different depths and hydrologic conditions (Huguet et al., 2007).

118 Degradation of GDGTs through the water and sediment columns potentially affects
119 the TEX_{86} values (Huguet et al., 2009). If this effect is relatively large, it introduces

120 error into palaeotemperature estimations that are based on TEX_{86}. GDGT degradation
121 through the water column is evaluated based on the decreasing trend of sinking flux
122 with increasing depth. Most sediment trap studies, however, have not detected this
123 decreasing trend because of interference by the lateral influx of allochthonous GDGTs
124 to deeper traps (e.g., Wuchter et al., 2006b). Furthermore, there is very little information
125 on the degradation rate of GDGTs at the water-sediment interface, aside from a few
126 studies (e.g., Sinninghe Damsté et al., 2002a). Evaluation of the preservation rate of
127 GDGTs at the sediment surface is required by methods such as the comparison of the
128 sinking fluxes of GDGTs through the water column and their accumulation rates in the
129 sediment at the same location.
130 In this study, we examined the seasonal and depth variations in GDGT flux and
131 molecular compositions of sinking particles. We conducted a time-series sediment trap
132 experiment at a mooring station (39°N, 147°E; Fig. 1) in the mid-latitude NW Pacific
133 from November 1997 to August 1999 to understand seasonality, sinking processes and
134 degradation of GDGTs in the water column and the influence on TEX_{86}. Analysis of the
135 underlying sediments was also conducted to evaluate the effects of GDGT degradation
136 at the water-sediment interface on TEX_{86}.
137
138 **2. Station WCT-2 and previous results**
139 The study site, station WCT-2, is located in the mixing zone between Oyashio and
140 Kuroshio waters (Fig. 1). Cold and warm mesoscale eddies from the Oyashio and
141 Kuroshio, respectively, develop in the mixing zone. The Oyashio–Kuroshio boundary is
142 displaced seasonally. The southern limit of the Oyashio stays at ~38.5°N in April,
143 gradually shifts northward to ~40°N until October, and then moves more rapidly

144 northward to ~41.5°N to December before gradually returning southward until April
145 (Data from Japan Meteorological Agency, http://www.data.kishou.go.jp/kaiyou/
146 db/hakodate/knowledge/oyashio.html.) The monthly mean SST ranges from ~9°C
147 (March) to ~24°C (August) and averages ~15°C (Fig. 2a; Conkright et al., 2002). The
148 seasonal SST change reflects both the latitudinal displacement of the Oyashio-Kuroshio
149 boundary and the development of thermal stratification. Thermal stratification develops
150 from summer to fall in this region (Fig. 2b). An ocean general circulation model study
151 indicated that the average surface current velocity was ~10 cm/sec (~8.6 km/day and
152 ~260 km/month) during winters at site WCT-2 (Nonaka et al., 2006); this velocity is
153 much lower than that of the Kuroshio Extension.

154 Two seasonal cycles were observed in both the compositions and the flux of
155 biogenic matter during the 21 months from November 1997 to August 1999 at station
156 WCT-2 (Mohiuddin et al., 2002; Yamamoto et al., 2007). Opal content ranged from
157 28% to 63% with an average of 48%, implying that diatom frustules are a major
158 component of the sinking particles at this site. The total fine fraction (< 1 mm diameter),
159 organic carbon, calcium carbonate, and opal fluxes showed strong seasonal variability
160 in traps at each depth. Organic carbon, calcium carbonate, and biogenic opal fluxes
161 began to increase in February–early March and reached a maximum in early May–early
162 July, abruptly decreased in late July, and remained nearly constant after August. Traps at
163 different depths showed similar variations. The biogenic fluxes in the middle and deep
164 traps exceeded those in the shallow trap from April to June, which was attributed to the
165 lateral influx of particles in deeper traps (Mohiuddin et al., 2002).

166 The alknone concentration and sinking flux also showed strong seasonal variability
167 in traps at each depth (Yamamoto et al., 2007). The alkenone concentration and sinking

flux increased abruptly in mid-March–April, showed multiple maxima in spring to fall. Traps at the different depths showed similar variations except for the interval between April and May 1999, when the alkenone fluxes in the middle and deep traps exceeded those in the shallow trap. The high alkenone flux from spring to fall corresponded to the high flux of *Emiliania huxleyi* (Yuichiro Tanaka, unpublished data), presumably reflecting the repeated blooms of *Emiliania huxleyi* in this station. Seasonal cycles in alkenone flux lagged behind those of the fluxes in the total fine fraction and bulk biogenic components by about one month. The time lag between bulk biogenic and alkenone fluxes was attributed to the ecological succession of the blooming of alkenone-producing coccolithophores after the blooming of diatoms (Yamamoto et al., 2007).

3. Samples and methods

3.1. Samples

Moored time-series sediment traps were employed at three different depths at the WCT-2 site (39°00'N, 147°00'E) in the western North Pacific from 19 November 1997 to 10 August 1999 (Table 1). The traps were set and recovered during the Western Pacific Environmental Assessment Study (WEST) CO_2 Ocean Sequestration for Mitigation of Climate Change (COSMIC) cruises in 1997, 1998, and 1999 aboard the R/V Daini Hakurei-maru (Mohiuddin et al., 2002). Sample cups at shallow and deep depths were replaced every 13 days from 19 November 1997 to 6 August 1998 and every 18 days from 26 August 1998 to 10 August 1999. The sample cups at middle depths were replaced every 22 days from 19 November 1997 to 10 August 1998 and every 30 days from 27 August 1998 to 10 August 1999. The cups were filled with 1%

192 $HgCl_2$ seawater (pH = ~7). Recovered particles were separated into a coarse fraction
193 (>1 mm diameter) and a fine fraction (<1 mm) by filtering. The coarse fraction was
194 made up of scoriae and swimmers. The fine fraction was collected on a membrane filter
195 (0.6 mm pore diameter), dried at 60°C for one day and milled using an agate mortar.
196 Scoriae were picked with tweezers during grinding.
197 The multiple core CMC18, 30 cm long, was taken at 39°00.0'N, 146°56.0'E, at a
198 depth of 5389 m during WEST COSMIC cruise NH99 of the R/V Daini Hakurei-maru
199 on 7 August 1999. The sediments consist of dark olive brown diatomaceous silty clay
200 from 0 to 10 cm deep and olive black diatomaceous clay with ash patches from 10 to 30
201 cm deep (Yamamoto et al., 2007). The core was sampled every 0.31 cm, and 10 samples
202 were selected at 0.62 cm interval for analysis.
203 The age model was created using the calendar ages converted from the AMS ^{14}C
204 ages of bulk organic matter in six sediment samples (1380–8000 ^{14}C yrs. BP) using
205 CALIB4.3 software and the marine98 calibration data set (Stuiver and Reimer, 1993)
206 with a 400-year global reservoir correction (Yamamoto et al., 2007).
207
208 *3.2. Analytical methods*
209 Lipids were extracted from the fine fraction by five 5-min rounds of
210 ultrasonication with 5 ml of dichloromethane-methanol (6:4), then concentrated and
211 passed through a short bed of Na_2SO_4 to remove water. The lipid extract was separated
212 into four fractions (F1: 3 ml of hexane; F2: 3 ml of hexane-toluene (3:1); F3: 4 ml of
213 toluene; F4: 3 ml of toluene-methanol (3:1)) by column chromatography (SiO_2 with 5%
214 distilled water; i.d., 5.5 mm; length, 45 mm).
215 An aliquot of F4 was trans-esterified with 1 ml 5% HCl/CH_3OH at 60 ˚C for 12 h

under N_2. The methylated lipids were supplemented with 2 ml distilled water and extracted (3x) with toluene. The extract was back washed (3x) with distilled water, passed through a short bed of Na_2SO_4, and separated into two fractions with SiO_2 column chromatography: F4-1 (acids), 4 ml toluene; F4-2 (alcohols), 3 ml toluene–CH_3OH (3:1). *n*-$C_{24}D_{50}$ was added as an internal standard to F4-1.

An aliquot of F4-2 was dissolved in hexane-2-propanol (99:1) and filtered. GDGTs were analyzed using high performance liquid chromatography-MS (HPLC-MS) with an Agilent 1100 HPLC system connected to a Bruker Daltonics micrOTOF-HS time-of-flight mass spectrometer. Separation was conducted using a Prevail Cyano column (2.1 x 150 mm, 3μm; Alltech) maintained at 30˚C following the method of Hopmans et al. (2000) and Schouten et al. (2007). Conditions were: flow rate 0.2 ml/min, isocratic with 99% hexane and 1% 2-propanol for the first 5 min followed by a linear gradient to 1.8% 2-propanol over 45 min. Detection was achieved using atmospheric pressure, positive ion chemical ionization-MS (APCI-MS). The spectrometer was run in full scan mode (*m/z* 500−1500). Compounds were identified by comparing mass spectra and retention times with those of GDGT standards (obtained from the main phospholipids of *Thermoplasma acidophilum* via acid hydrolysis) and those in the literature (Hopmans et al., 2000). Quantification was achieved by integrating the summed peak areas in the $(M+H)^+$ and the isotopic $(M+H+1)^+$ chromatograms and comparing these with the peak area of an internal standard (C_{46} GDGT; Patwardhan and Thompson, 1999) in the $(M+H)^+$chromatogram, according to the method of Huguet et al. (2006a). The correction value of ionization efficiency between GDGTs and the internal standard was obtained by comparing the peak areas of *T. acidophilum*-derived mixed GDGTs and C_{46} GDGT in known amounts. The standard deviation of a replicate analysis

was 3.0% of the concentration for each compound. TEX_{86} and TEX_{86}^{H} (applicable to warm water) were calculated from the concentrations of GDGT-1, GDGT-2, GDGT-3 and a regioisomer of crenarchaeol using the following expressions (Schouten et al., 2002; Kim et al., 2010):

$$TEX_{86} = ([GDGT\text{-}2]+[GDGT\text{-}3]+[Crenarchaeol\ regioisomer])/([GDGT\text{-}1]+[GDGT\text{-}2]+[GDGT\text{-}3]+[Crenarchaeol\ regioisomer])$$

$$TEX_{86}^{H} = \log (TEX_{86})$$

TEX_{86}^{L}, applicable in cooler water, was calculated from the concentrations of GDGT-1, GDGT-2 and GDGT-3 using the following expression (Kim et al., 2010):

$$TEX_{86}^{L} = \log \{[GDGT\text{-}2] / ([GDGT\text{-}1]+[GDGT\text{-}2]+[GDGT\text{-}3])\}$$

Temperatures were calculated according to the following equations based on a global core top calibration (Kim et al., 2010):

$$T = 68.4\ TEX_{86}^{H} + 38.6 \quad (\text{when } T > 15°C)$$

$$T = 67.5\ TEX_{86}^{L} + 46.9 \quad (\text{when } T < 15°C)$$

where T = temperature [°C]; analytical accuracy was 0.45 °C in our laboratory.

Calculation of mass accumulation rate in core CMC18

263 The accumulation rate of GDGTs (GDGT AR) was calculated according to the
264 following formula:
265
266 GDGT AR ($\mu g/cm^2/kyr$) = GDGTs ($\mu g/g$-sed.) x DBD (g/cm^3) x LSR (cm/kyr)
267
268 where AR is the accumulation rate, DBD is the dry bulk density, and LSR is the linear
269 sedimentation rate derived from ^{14}C-based age-depth model. The DBD was obtained by
270 the following regression equation between ten measured DBDs and depth (Tatsuo
271 Fukuhara, unpublished data):
272
273 DBD (g/cm^3) = 0.00780 x Depth (cm) + 0.324
274
275 *3.3. Estimation of chlorophyll concentration and net primary production*
276 Surface chlorophyll-a concentration at the WCT-2 site was extracted from monthly
277 9 km data of NASA SeaWiFS standard mapped image and take a median values of 3 x 3
278 pixels. Integrated primary production was calculated with a modified version (Kameda
279 and Ishizaka, 2005) of vertically generalized production model (Behrenfeld and
280 Falkowski, 1997) using SeaWiFS SMI monthly photosynthetically available radiation
281 and AVHRR Pathfinder monthly nighttime SST.
282
283 **4. Results**
284 *4.1. Sediment trap*
285 The concentration of isoprenoid GDGTs, consisting of caldarchaeoal (GDGT-0),
286 GDGT-1, GDGT-2, GDGT-3, crenarchaeol, and crenarchaeol regioisomer, varied from

40 to 218 μg g^{-1} in the shallow trap, from 36 to 113 μg g^{-1} in the middle trap and from 21 to 102 μg g^{-1} in the deep trap and showed strong seasonal variability in traps at each depth (Fig. 3a). The GDGT concentration gradually decreased from November 1997 to June 1998, increased from early July to late September, and then gradually decreased to May and June in 1999 (Fig. 3a). Traps at the different depths showed similar variations except for the interval between July and November 1998, when the GDGT concentrations in the shallow trap were two times larger than those in the middle and deep traps.

The sinking flux of GDGTs varied from 4 to 41 μg m^{-2} d^{-1} in the shallow trap, from 4 to 27 μg m^{-2} d^{-1} in the middle trap and from 1 to 27 μg m^{-2} d^{-1} in the deep trap (Fig. 3b). The sinking flux showed strong temporal variability in the shallow traps (~1300 m), whereas the sinking fluxes in the deeper traps (~2500–4800 m) did not vary in harmony with that in the shallow trap. In 1998, the GDGT concentration and sinking flux in the shallow trap increased abruptly in late June/early July and showed maxima in late June/early July, September, early November, and December/January 1999. In 1999, after the maximum in February, GDGT flux was relatively low. The fluxes in the middle and deep traps were relatively unchanged and showed a maximum in late April-early May which exceeded that in the shallow trap (Fig. 3b).

The TEX_{86}^{H}- and TEX_{86}^{L}-based temperatures calculated using the core-top calibrations of Kim et al. (2010) varied from 9°C to 19°C and from 11°C to 21°C, respectively, in the shallow site, from 11°C to 16°C and from 14°C to 18°C in the middle site, and from 10°C to 16°C and from 11°C to 18°C in the deep site (Figs. 3c and 3d). TEX_{86}^{H}-based temperatures were 0–3°C lower than TEX_{86}^{L}-based temperatures. The TEX_{86}^{H}- and TEX_{86}^{L}-based temperatures fluctuated from November 1997 to June

311 1998, decreased in early July 1998 and were constantly low from early July 1998 to
312 early November 1998, and then increased in late November 1998 and fluctuated
313 thereafter (Figs. 3c and 3d). This change was different from the changes seen in SSTs
314 (Figs. 3c and 3d, Integrated Global Ocean Services System [IGOSS] weekly SST;
315 Reynolds et al., 2002): the TEX_{86}^{H}- and TEX_{86}^{L}-based temperatures were generally
316 higher than the SST from January to May, whereas it was lower than the SST from
317 May–June to December.

318 The relative abundance of caldarchaeol and crenarchaeol (Cald/Cren ratio) is
319 assumed to respond to SST (Schouten et al., 2002). The Cald/Cren ratio varied from 0.8
320 to 1.5. The maximum appeared in late July 1998 and corresponded to a low TEX_{86}^{H}- or
321 TEX_{86}^{L}-based temperature (Fig. 3e). The minimum appeared in early December 1998
322 and corresponded to high TEX_{86}^{H}- and TEX_{86}^{L}-based temperatures (Figs. 3c–3e). The
323 ratio had a significant negative correlation with TEX_{86}^{H}- and TEX_{86}^{L}-based temperatures
324 (both $r = -0.69$).

325

326 *4.2. Core CMC18*

327 The GDGT concentration was highest at the core top, decreased abruptly
328 downwards until 1.6 cm (~1.6 ka) and showed a maximum at 9.1 cm (~2.8 ka) (Fig. 4).
329 The alkenone GDGT AR showed a similar changing pattern with that of GDGT
330 concentration, but it showed an enhanced peak interval from 4.1 to 9.1 cm deep (from
331 ~2.3 ka to ~2.8 ka), and the maximum appeared at 6.6 cm (Fig. 4) due to the high linear
332 sedimentation rate in this interval.

333 TEX_{86}^{H}- and TEX_{86}^{L}-based temperatures at the core top were 16.8°C and 16.3°C,

334 respectively, which are 1–2°C higher than the mean annual SST at this site (15°C,
335 Conkright et al., 2002). TEX_{86}^{H}- and TEX_{86}^{L}-based temperatures varied between 15.6°C
336 and 19.0°C and between 12.9°C and 17.9°C, respectively, during the last 5.9 ka (Fig. 4).
337
338 *4.3. Satellite-based surface chlorophyll concentration and estimated net primary*
339 *production*
340 Satellite-based surface chlorophyll concentration at the study site showed a
341 seasonal cycle with lower values from July to October (Fig. 5a). The low surface
342 chlorophyll concentrations from summer to fall presumably reflect both the decrease of
343 primary production and the deepening of chlorophyll maximum in the water column.
344 Observations at the A-17 site (39°N, 146.75°E) of A-line monitored by the Fishery
345 Research Agency of Japan revealed the decrease of surface water chlorophyll
346 concentration and the deepening of chlorophyll maximum in early July 1998 (Fig. 4a;
347 Fishery Research Agency of Japan, 2012), supporting this interpretation. Estimated net
348 primary production (NPP) basically showed a similar seasonal pattern with chlorophyll
349 concentration, but the maximal peaks in June shifted one or two months later than the
350 peaks of chlorophyll concentration in April and May, because NPP includes subsurface
351 production enhanced in summer.
352
353 **5. Discussion**
354 *5.1. Season of export production of isoprenoid GDGTs*
355 In the shallow trap, the sinking flux of GDGT showed maxima from May 1998 to
356 February 1999 (Fig. 5c). The maximal peak of GDGT sinking flux corresponded to the
357 peak of the sinking fluxes of organic carbon, opal and lithogenic material (Figs. 5b and

358 5c). The sinking flux of GDGTs was better correlated with those of organic carbon ($r = 0.80$, $p<0.01$), opal ($r = 0.59$, $p<0.01$), lithogenic material ($r = 0.68$, $p<0.01$), and alkenones ($r = 0.50$, $p<0.05$) than $CaCO_3$ ($r = 0.31$) in the shallow trap. This implies that GDGTs sank with the main components of organic matter which are associated with diatom frustules and lithogenic material.

363 Changes in the sinking fluxes of biogenic opal, $CaCO_3$, organic carbon, and GDGTs were generally consistent with changes in chlorophyll concentration and NPP; the sinking fluxes are higher when chlorophyll concentration and NPP were higher (Figs 5a and 5b). Exceptionally, the highest sinking fluxes of opal, organic carbon, GDGTs, and alkenones were found in early July 1998, but surface chlorophyll concentration NPP were relatively low in this period. It is not clear at this stage whether this was caused by the time lag between the production and sinking of biogenic materials or the subsurface production of primary producers.

371 The season of GDGT production in the marine environment is still not clear. Wuchter et al. (2005), Herfort et al. (2006), and Pitcher et al. (2011) reported that GDGT concentrations in surface water were higher in winter in the North Sea and suggested that Thaumarchaeota thrive in winter because they do not need to compete with phytoplankton for NH_3. Wuchter et al. (2006b) showed that the sinking flux of GDGTs was higher in the periods of enhanced primary production in the Arabian Sea and interpreted that the high sinking flux of GDGTs during high marine production was not necessarily caused by higher production of Thaumarchaeota, but by more efficient food web-based scavenging of archaeal cells, attached to aggregates or in faecal pellets. Huguet et al. (2007) found that the sinking flux of GDGTs was reduced in non-upwelling periods in the Santa Barbara Basin. They proposed that reduced primary

382 production resulted in a decrease in ammonia availability and lower Thaumarchaeota
383 productivity because components of the Thaumarchaeota are nitrifiers (Könneke et al.,
384 2005; Wuchter et al., 2006a) and use ammonia, produced by the decay of phytoplankton
385 and zooplankton, as an energy source.

386 The present study demonstrated that the sinking flux of GDGTs was enhanced with
387 increasing fluxes of organic matter, diatom frustules and lithogenic materials (Figs. 5b
388 and 5c). This is attributed either to enhanced production of Thaumarchaeota during the
389 phytoplankton bloom or to that the scavenging of GDGTs is enhanced when the organic
390 particulate flux increases after the phytoplankton bloom. In the former case,
391 Thaumarchaeota production would be supported by the supply of ammonia and labile
392 organic compounds derived from decay of plankton. In the latter case, the sinking of
393 GDGTs would be triggered by phytoplankton blooms that accelerated the attachment
394 and entrainment of Thaumarchaeota cells to larger particles. The latter case is more
395 likely to explain the disagreement between TEX_{86}-based temperatures and SSTs
396 observed in this study.

397

398 *5.2. Depth changes of GDGT sinking fluxes*

399 GDGT concentrations in the total fine fraction varied synchronously at three
400 depths from approximately 1300 m to 4800 m (Fig. 3a). The Cald/Cren ratio also
401 showed synchronous variations at the three different depths (Fig. 3e). The sampling
402 interval was 13 days and no significant time lag was seen in the GDGT concentrations
403 and the Cald/Cren ratio, implying that particles sank ~3400 m within 13 days; the
404 sinking velocity below ~1300 m was calculated to be higher than 260 m d^{-1}. This
405 velocity is in the range of those of faecal pellets and marine snow (Honjo and Roman,

406 1978; Small et al., 1979; McCave, 1984; Asper, 1987). Recently, settling velocity
407 sediment trap experiments revealed that a large proportion of particulate organic matter
408 sinks 200–500 m d^{-1} in the north-western Mediterranean Sea (Armstrong et al., 2009;
409 Wakeham et al., 2009). This range is consistent with the velocity estimated in this study.
410 The annual average sinking fluxes of GDGTs were 12.6–16.4 μg m^{-2} d^{-1} in the
411 shallow trap, 6.8–14.2 μg m^{-2} d^{-1} in the middle trap, and 6.2–7.8 μg m^{-2} d^{-1} in the deep
412 trap (Table 2). The range of sinking flux is of the same magnitude as that in the Arabian
413 Sea (4–12 μg m^{-2} d^{-1}; Wuchter et al., 2006b) but is lower than that in the Santa Barbara
414 Basin (~100 μg m^{-2} d^{-1}; Huguet et al., 2007).
415 The annual average sinking flux of GDGTs decreased with increasing depth (Fig.
416 6). The GDGT flux was almost identical between the NH97 and NH98 intervals. Nearly
417 synchronous variations in the Cald/Cren ratio, TEX_{86}^{H}, and TEX_{86}^{L} at the traps of
418 different depths (Figs. 3c–3d) suggest that the incorporation of GDGTs into sinking
419 particles in the middle and deep water column is not significant, and that the sinking
420 particles are mostly transported from the shallow water column. Assuming that the
421 sinking rates are constant in the entire middle and deep water column, and the GDGTs
422 are lost at a constant degradation rate during sinking, the relationship between sinking
423 flux and depth is expressed by the following formula:
424
425 $$F_Z = F_0 e^{-kZ}$$
426
427 where Z is depth (m), F_Z is the sinking flux at depth Z, F_0 is the presumed extrapolated
428 sinking flux at the sea surface, and k is the decomposition rate constant with depth. The
429 half-depth ($Z_{1/2}$), defined as the depth range over which half of material is lost, is

calculated by the following equation (Wakeham and Lee, 1993):

$$Z_{1/2}\ (m) = \ln 2/k = 0.693/k$$

Table 3 shows the calculated $Z_{1/2}$, F_0, and F_{5389} (the presumed extrapolated sinking flux at the sea bottom). The half-depths of GDGT flux in the NH97 and NH98 intervals were 3349 m and 3108 m, respectively. The half-depth of GDGT was the same level as that of organic carbon (3655–3738 m; Yamamoto et al., 2007) and higher than that of alkenones (1572–1982 m; Yamamoto et al., 2007). This result indicates that GDGTs are well preserved during sinking in the water column.

5.3. Preservation efficiency of GDGTs at the sediment surface

A comparison between GDGT fluxes at the bottom of the water column and the core-top GDGT AR of Core CMC18 provides a measure of the preservation efficiency of GDGTs at the water-sediment interface. The GDGT fluxes at the bottom of the water column (F_{5389} in Table 3) as estimated by the sediment trap were 5.0 and 6.7 μg m^{-2} d^{-1} during the NH97 and NH98 sampling intervals, respectively. The NH97 interval did not cover an entire year and did not include the autumn high flux season; thus the GDGT flux was underestimated. The NH98 interval covered an entire year but also included the short period of lateral influx into deeper traps (Yamamoto et al., 2007); thus the GDGT flux was overestimated, although the effect of lateral influx was not significant because the period was short (36 days). Because the core-top GDGT AR of Core CMC18 was 2.40 μg cm^{-2} d^{-1} (0.065 μg m^{-2} d^{-1}; Fig. 4), the preservation efficiency of GDGTs is estimated to be 1.0–1.3%. This preservation efficiency was about one third of

454 that of alkenones (2.7–5.2%; Yamamoto et al., 2007) and one fifth of that of organic
455 carbon (5.5–6.7%; Yamamoto et al., 2007) at the same site.

456 Prahl et al. (2000) estimated the preservation rates of alkenones (0.8%) and organic
457 carbon (3.3%) at the sediment surface in the central Arabian Sea, based on their
458 concentrations normalized to Al for sediment trap particles and bottom sediments.
459 Wakeham et al. (2002) compared the accumulation rates of organic carbon and
460 biomarkers in the bottom sediments with their sinking fluxes at the deepest sediment
461 traps in the Arabian Sea and estimated that the preservation rates of organic carbon and
462 $C_{37:2}$ alkenone are 3.3–24.0% and 0.1–44.7%, respectively. Sinninghe Damsté et al.
463 (2002a) estimated the relative preservation efficiencies of biomarkers in oxic, suboxic
464 and anoxic environments by comparing their accumulation rates at the same horizon at
465 different locations in the Arabian Sea. They showed that terrestrial n-alkanes are more
466 resistant to degradation than GDGTs and alkenones which are more refractory than
467 steroids. Mollenhauer et al. (2008) suggested that crenarchaeaol is more efficiently
468 degraded during lateral transport in oxygen replete environments than are alkenones
469 based on their radiocarbon concentrations. Yamamoto and Polyak (2009) estimated the
470 first-order decomposition rate constants of organic carbon (1.1×10^{-5} yr^{-1}), C_{25}–C_{33}
471 n-alkanes (1.0×10^{-5} yr^{-1}), isoprenoid GDGTs (2.5×10^{-5} yr^{-1}), and branched GDGTs
472 (2.0×10^{-5} yr^{-1}), based on the decreasing trends of their concentrations in an Arctic
473 sediment core. These studies indicated that most GDGTs are remineralised at the
474 sediment surface in an oxic environment and that they are less refractory than total
475 organic carbon and n-alkanes and more refractory than steroids. The estimated
476 preservation rates of GDGTs in this study are consistent with this perspective.
477

478 *5.4. Seasonal variation in TEX_{86}*

479 The changes in TEX^{H}_{86}- and TEX^{L}_{86}-based temperatures were different from those
480 of the contemporary SST (Fig. 5d). The TEX^{H}_{86}- and TEX^{L}_{86}-based temperatures were
481 lower than the SST from May to December, whereas they were higher than the SST
482 from December to May (Fig. 5d). Disagreement in the seasonal pattern between the
483 TEX_{86}-based temperature of sinking particles and the contemporary SST was reported
484 in the traps below 1500 m in the Arabian Sea (Wuchter et al., 2006b) and in the Santa
485 Barbara Basin (Huguet et al., 2007). The former case was explained by a
486 homogenization of the TEX_{86} SST signal carried by particles from a large area (Wuchter
487 et al., 2006b). The latter case was attributed to a complex combination of the
488 contributions of GDGTs produced in different depths and hydrologic conditions
489 (Huguet et al., 2007).

490 At the present study site, a similar pattern was observed in seasonal changes in the
491 $U^{K'}_{37}$-based temperature (Fig. 5d; Yamamoto et al., 2007), which showed parallel
492 changes at each depth. The $U^{K'}_{37}$-based temperature decreased gradually after October
493 during the low alkenone flux period, abruptly decreased in April at the beginning of the
494 high alkenone flux period, was minimized in April–May, and then increased until
495 September. This change was different from that observed in the SSTs. The $U^{K'}_{37}$-based
496 temperatures were lower than the contemporary SST during the periods of high
497 alkenone flux from spring to fall, suggesting alkenone production in a well-developed
498 thermocline (shallower than 30 m). During low alkenone flux periods from fall to spring,
499 the $U^{K'}_{37}$-based temperatures were nearly constant and were higher than the
500 contemporary SSTs. The nearly constant carbon isotopic ratios of $C_{37:2}$ and $C_{38:2}$
501 alkenones suggest that the source of alkenones was unchanged and that the alkenones

502 produced in early fall were suspended in the surface water until sinking (Yamamoto et
503 al., 2007).

504 From May to December, the TEX^{H}_{86}- and TEX^{L}_{86}-based temperatures were a
505 maximum of 9–12°C lower than the contemporary SST (Fig. 5d). Because thermal
506 stratification is developed in summer and fall in the western North Pacific (Fig. 2), the
507 TEX^{H}_{86}- and TEX^{L}_{86}-based temperatures corresponded to the temperatures at the
508 thermocline. When we recovered the sediment traps at the end of the first sampling
509 interval (NH97) in August 1998, we obtained a snapshot profile of water temperatures
510 and chlorophyll concentrations in the water column at the study site. The depth profile
511 indicates that the TEX^{H}_{86}- and TEX^{L}_{86}-based temperatures (9.4°C and 12.7°C,
512 respectively) in the shallow trap corresponded to the water temperatures at 70 m and 40
513 m depths, respectively (Fig. 7). This correspondence suggests that the depth of GDGT
514 production was 40–70 m if there was no time lag between GDGT production and
515 sinking. The estimated depths overlap depths showing high chlorophyll concentrations
516 (30–70 m; Fig. 7). If there was a time lag, the GDGT production depth would be
517 shallower.

518 From December to May, the TEX^{H}_{86}- and TEX^{L}_{86}-based temperatures were a
519 maximum of 8–9°C higher than the contemporary SST. A similar pattern was observed
520 in $U^{K'}_{37}$-based temperatures during the low alkenone flux period at the study site (Fig.
521 5d) and was attributed to the gradual sinking of alkenones that had been produced in the
522 previous period of high alkenone flux. This interpretation is applicable to the case of
523 TEX_{86}, but the Cald/Cren ratio varied significantly from 0.9 to 1.4 during this period
524 (Fig. 3e), suggesting the successive change in GDGT composition. This change is

525 probably caused by the heterogeneous distribution of GDGTs in the surface water pool,
526 the successive addition of newly-produced GDGTs, and/or the lateral advection of
527 GDGTs by strong surface currents. An ocean general circulation model study indicated
528 that the average of surface current velocity was ~10 cm/sec (~8.6 km/day and ~260
529 km/month) during winters at site WCT-2 (Nonaka et al., 2006). If particle residence
530 times are long enough, the warm-water detrital GDGTs could be supplied by the
531 Kuroshio Current in winter to spring. It is not clear which process caused
532 TEX_{86}-derived temperatures to be higher than SSTs from winter to spring. Further case
533 studies are necessary to fully understand the phenomenon.
534
535 *5.5. Depth variations in TEX_{86}*
536 The flux-weighted average TEX_{86}^{H}- and TEX_{86}^{L}-based temperatures were constant
537 with depth (13.5–14.2°C, average 13.8°C and 15.4–16.3°C, average 15.9°C,
538 respectively; Fig. 8 and Table 2) and ~2 to 0°C lower than mean annual SST in 1998
539 (15.9°C; Reynolds et al., 2002). Wuchter et al. (2005) reported a high concentration of
540 GDGTs in POM in the deep water column below 100 m and stated that the
541 TEX_{86}-derived temperatures of POM at all depths correspond to SSTs. On the basis of
542 this observation, they concluded that the GDGTs produced in surface waters were
543 preferentially delivered to the deeper water column by grazing and repackaging in
544 larger particles. Our results show that the flux-weighted average TEX_{86} of sinking
545 particle reflects SST and/or the seasonal thermocline temperature that is affected by SST,
546 like the TEX_{86} of suspended POM does. This finding implies that the particles that give
547 a SST signal are delivered downward, and the suspended POM originated from such
548 sinking particles, which supports the hypothesis of Wuchter et al. (2005). The constant

549 TEX_{86} at different depths implies that TEX_{86} is not affected by degradation in the water
550 column.

551 The flux-weighted average TEX_{86}^{H}- and TEX_{86}^{L}-based temperatures are 2.6–3.3°C
552 and 0–0.9°C lower than the TEX_{86}^{H}- and TEX_{86}^{L}-based temperatures at the core top
553 (16.8°C and 16.3°C), respectively. In the case of TEX_{86}^{H}, the difference in estimated
554 temperatures between traps and core-top sediment (2.6–3.3°C) is larger than the error of
555 TEX_{86}^{H} palaeothermometry (2.5°C; Kim et al., 2010), whereas in the case of TEX_{86}^{L},
556 the difference (0–0.9°C) corresponds to the error. Surface sediment was mixed with
557 subsurface sediments by bioturbation and may contain a preindustrial signal of cooler
558 temperature than contemporary temperature, and the TEX_{86}-based temperature at the
559 core-top sample is possibly biased in the cooler direction. Even considering this bias,
560 TEX_{86}^{L} shows a better agreement between traps and the bottom sediment than TEX_{86}^{H}.
561 Whether the degradation at the water-sediment interface did not affect the TEX_{86} (Kim
562 et al., 2009) or increased the TEX_{86} (Huguet et al., 2009) depends on the applied
563 parameter TEX_{86}^{H} or TEX_{86}^{L}. Kim et al. (2010) recommended that TEX_{86}^{H} be used in
564 warmer temperature regions (>15°C) and TEX_{86}^{L} in cooler temperature regions
565 (<15°C). In this study, the flux-weighted average TEX_{86}^{L}-based temperatures in
566 sediment traps were more consistent with values in the bottom sediment than were
567 TEX_{86}^{H}-based temperatures. This suggests that TEX_{86}^{L} is more reliable than TEX_{86}^{H} in
568 the studied region. The TEX_{86}^{L}-based temperatures in sediment traps (15.4–16.3°C) and
569 the bottom sediment (16.3°C) correspond to temperatures at the depth range of 0–40 m
570 from July to November in the study site.
571

572 **6. Conclusions**

573 GDGT and TEX_{86} analyses of sediment trap and bottom sediment samples
574 revealed that flux-averaged TEX_{86}-based temperatures were 1) nearly constant in
575 sediment traps of different depths, 2) agreed with the value of the bottom sediments,
576 and 3) corresponded to water temperatures at 0–40 m depth from July to November,
577 suggesting that the temperature signal was propagated through the water column by the
578 sinking of GDGTs. The analyses also indicated a rapid vertical transport of GDGTs to
579 deeper water (> 260 m d^{-1}) and the relatively refractory nature of GDGTs during sinking
580 (the half-depth = 3108–3349 m) and at the sediment surface (preservation efficiency =
581 1.0–1.3%). These findings suggest that the signal of GDGTs produced in surface or
582 near-surface water is preserved during vertical transport and thus propagated to the
583 sediment surface.

584

585 Acknowledgments: We thank Kazuko Hino, Etsuko Kamata (Geological Survey of
586 Japan), Tatsufumi Okino and Keiko Ohnishi (Hokkaido University) for analytical
587 assistance in the laboratory. Special thanks are due to the members of NEDO
588 WEST-COSMIC “Carbon Dioxide Ocean Sequestration for Mitigation of Climate
589 Change” and the staff of the General Environmental Technos Co. LTD. for sampling and
590 their helpful discussions. We also thank Jan W. de Leeuw and three anonymous
591 reviewers for editorial and constructive comments. The study was supported by a
592 grant-in-aid for Scientific Research (A) the Japan Society for the Promotion of Science,
593 No. 19204051 (to M.Y.).

594

595 **References**

596 Agogué, H., Brink, M., Dinasquet, J., Herndl, G.J., 2008. Major gradients in putatively
597 nitrifying and non-nitrifying Archaea in the deep North Atlantic. Nature, 456,
598 788–792.
599 Armstrong, R.A., Peterson, M.L., Lee, C., Wakeham, S.G., 2009. Settling velocity
600 spectra and the ballast ratio hypothesis. Deep-Sea Research II, 56, 1470–1478.
601 Asper, V.J., 1987. Measuring the flux and sinking speed of marine snow aggregates.
602 Deep-Sea Research Part A 34, 1–17.
603 Baltar, F., Aristegui, J., Gasol, J.M., Hernandez-Leon, S. Herndl, G.J., 2007. Strong
604 coast-ocean and surface-depth gradients in prokaryotic assemblage structure and
605 activity in a coastal transition zone region. Aquatic Microbial Ecology, 50, 63–74.
606 Behrenfeld, M.J., Falkowski , P.G., 1997. Photosynthetic rates derived from
607 satellite-based chlorophyll concentration. Limnology and Oceanography 42, 1–20.
608 Beman, J.M., Popp, B.N., Francis, C.A., 2008. Molecular and biogeochemical evidence
609 for ammonia oxidation by marine Crenarchaeota in the Gulf of California. The ISME
610 Journal, 2, 429–441.
611 Blainey, P.C., Mosier, A.C., Potanina, A., Francis, C.A., Quake, S.R., 2011. Genome of
612 a low-salinity ammonia-oxidizing Archaeon determined by single cell and
613 metagenomic analysis. PLoS ONE, 6, 1–12.
614 Brochier-Armanet, C., Boussau, B., Gribaldo, S., Forterre, P., 2008. Mesophilic
615 crenarchaeota: proposal for a third archaeal phylum, the Thaumarchaeota. Nature
616 Reviews Microbiology, 6, 245–252.
617 Conkright, M.E., et al. 2002. World Ocean Atlas 2001: Objective Analyses, Data
618 Statistics, and Figures, CD-ROM Documentation. National Oceanographic Data
619 Center, Silver Spring, MD, 17 pp.

620 Coolen, M.J.L., Abbas, B., van Bleijswijk, J., Hopmans, E.C., Kuypers, M.M.M.,
621 Wakeham, S.G., Sinninghe Damsté, J.S., 2007. Putative ammonia-oxidizing
622 Crenarchaeota in suboxic waters of the Black Sea: a basin-wide ecological study
623 using 16S ribosomal and functional genes and membrane lipids. Environmental
624 Microbiology, 9, 1001–1016.
625 Fishery Research Agency of Japan, 2012. A-line data home page,
626 http://hnf.fra.affrc.go.jp/a-line/.
627 Hallam, S.J., Mincer, T.J., Schleper, C., Preston, C.M., Roberts, K., Richardson, P.M.,
628 DeLong, E.F., 2006. Pathway of carbon assimilation and ammonia oxidation
629 suggested by environmental genomic analyses of marine Crenarchaeota. PLoS
630 Biology, 4, 520–536.
631 Herfort, L., Schouten, S., Boon, J.P., Sinninghe Damsté, J.S., 2006. Application of the
632 TEX_{86} temperature proxy to the southern North Sea. Organic Geochemistry 37,
633 1715–1726.
634 Herndl, G.J., Reinthaler, T.R., Teira, E., van Aken, H., Veth, C., Pernthaler, A.,
635 Pernthaler, J., 2005. Contribution of Archaea to total prokaryotic production in the
636 deep Atlantic Ocean. Applied and Environmental Microbiology 71, 2303–2309.
637 Honjo, S., Roman, M.R., 1978. Marine copepod fecal pellets: Production, Preservation
638 and Sedimentation. Journal of Marine Research 36, 45–57.
639 Hopmans, E.C., Schouten, S., Pancost, R., van der Meer, M.T.J., Sinninghe Damsté, J.S.,
640 2000. Analysis of intact tetraether lipids in archaeal cell material and sediments by
641 high performance liquid chromatography/atmospheric pressure chemical ionization
642 mass spectrometry. Rapid Communications in Mass Spectrometry 14, 585–589.
643 Huguet, C., Hopmans, E.C., Febo-Ayala, W., Thompson, D.H, Sinninghe Damsté, J.S.,

644 Schouten, S., 2006a. An improved method to determine the absolute abundance of
645 glycerol dibiphytanyl glycerol tetraether lipids. Organic Geochemistry 37,
646 1036–1041.
647 Huguet, C., Kim, J.-H., Sinninghe Damsté, J.S., Schouten, S., 2006b. Reconstruction of
648 sea surface temperature variations in the Arabian Sea over the last 23 kyr using
649 organic proxies (TEX_{86} and $U^{K'}_{37}$). Paleoceanography 21, PA300S.
650 Huguet, C., Schimmerlmann, A., Thunell, R., Lourens, L.J., Sinninghe Damsté, J.S.,
651 Schouten, S., 2007. A study of the TEX_{86} paleothermometer in the water column and
652 sediments of the Santa Barbara basin, Califrnia. Paleoceanography 22, PA3203.
653 Huguet, C., Kim, J.-H., de Lange, G.J., Sinninghe Damsté, J.S., Schouten, S., 2009.
654 Effects of long term oxic degradation on $U^{K'}_{37}$, TEX_{86} and BIT organic proxies.
655 Organic Geochemistry, 40, 1188–1194.
656 Ingalls, A.E., Huguet, C., Truxal, L.T., 2012. Distribution of intact and core membrane
657 lipids of archaeal glycerol dialkyl glycerol tetraethers among size-fractionated
658 particulate organic matter in Hood Canal, Puget Sound. Applied and Environmental
659 Microbiology, 78, 1480–1490.
660 Karner, M.B., DeLong, E.F., Karl, D.M., 2001. Archaeal dominance in the mesopelagic
661 zone of the Pacific Ocean. Nature 409, 507–510.
662 Kameda, T., Ishizaka, J., 2005. Size-fractionated primary production estimated by a
663 two-phytoplankton community model applicable to ocean color remote sensing.
664 Journal of Oceanography 61, 663–672.
665 Könneke, M., Bernhard, A.E., de la Torre, J.R., Walker, C.B., Waterbury, J.B., Stahl,
666 D.A., 2005. Isolation of an autotrophic ammonia-oxidizing Archaeon. Nature 437,
667 543–546.

668 Kim, J-H., Schouten, S., Hopmans, E. C., Donner, B., Sinninghe Damsté, J.S., 2008.
669 Global sediment core-top calibration of the TEX_{86} paleothermometer in the ocean.
670 Geochimica et Cosmochimica Acta, 72, 1154–1173.
671 Kim, J-H., Huguet, C., Zonneveld, K.A.F., Versteegh, G.J.M., Roeder, W., Sinninghe
672 Damsté, J.S., Schouten, S., 2009. An experiment field study to test the stability of
673 lipids used for the TEX_{86} and $U^{K'}_{37}$ paleothermometers. Geochimica et
674 Cosmochimica Acta, 73, 2888–2898.
675 Kim, J-H., van der Meer, J., Schouten, S., Helmke, P., Willmott, V., Sangiorgi, F., Koc,
676 N., Hopmans, E.C., Sinninghe Damsté, J.S., 2010. New indices and calibrations
677 derived from the distribution of crenarchaeal isoprenoid tetraether lipids:
678 Implications for past sea surface temperature reconstructions. Geochimica et
679 Cosmochimica Acta 74, 4639–4654.
680 Lee, K.-E., Kim, J.-H., Wilke, I., Helmke, P., Schouten, S., 2008. A study of the
681 alkenone, TEX_{86}, and planktonic foraminifera in the Benguela Upwelling System:
682 Implications for past sea surface temperature estimates. Geochemistry Geophysics
683 Geosystems 9, Q10019.
684 Lopes dos Santos, R., Prange, M., Castañeda, I.S., Schefuß, E., Mulitza, S., Schulz, M.,
685 Niedermeyer, E.M., Sinninghe Damsté, J.S., Schouten, S., 2010. Glacial–interglacial
686 variability in Atlantic meridional overturning circulation and thermocline
687 adjustments in the tropical North Atlantic. Earth and Planetary Science Letters 300,
688 407–414.
689 McCave, I.N., 1984. Size spectra and aggregation of suspended particles in the deep
690 ocean. Dee-Sea Research Part A 31, 329–352.

691 Mohiuddin, M.M., Nishimura, A., Tanaka, Y., Shimamoto, A., 2002. Regional and
692 interannual productivity of biogenic components and planktonic foraminiferal fluxes
693 in the northwestern Pacific Basin. Marine Micropaleontology 45, 57–82.
694 Mollenhauer, G., Eglinton, T.I., Hopamans, E.C., Sinninghe Damsté, 2008. A
695 radiocarbon-based assessment of the préservation characteristics of crenarchaeol and
696 alkenone from continental margin sédiments. Organic Geochemistry, 39, 1039–1045.
697 Murray, A.E., Blakis, A., Massana, R., Strawzewski, S., Passow, U., Alldredge, A., De
698 Long, E.F., 1999. A time series assessment of planktonic archaeal variability in the
699 Santa Barbara Channel. Aquatic Microbial Ecology 20, 129–145.
700 Nonaka, M., Kawamura, H., Tanimoto, Y., Kagimoto, T, Sasaki, H., 2006. Decadal
701 variability in the Kuroshio-Oyashio Extension simulated in an eddy-resolving
702 OGCM. Journal of Climate 19, 1970–1989.
703 Ouverney, C.C., Fuhrman, J.A., 2000. Marine planktonic Archaea take up amino-acids.
704 Applied Environmental Microbiology 66, 4829–4833.
705 Park, B.-J., Park, S.-J., Yoon, D.-N., Schouten, S., Sinninghe Damsté, J.S., Rhee, S.-K.,
706 2010. Cultivation of autotrophic ammonia-oxidizing Archaea from marine sediments
707 in coculture with sulfur-oxidizing bacteria. Applied and Environmental Microbiology,
708 76, 7575–7587.
709 Patwardhan, A.P., Thompson, D.H., 1999. Efficient synthesis of 40- and 48-membered
710 tetraether macrocyclic bisphosphocholines. Organic Letters 1, 241–243.
711 Pitcher, A., Wuchter, C.W., Siedenberg, K., Schouten, S., Sinninghe Damsté, J.S., 2011.
712 Crenarchaeol tracks winter blooms of ammonia-oxidizing Thaumarchaeota in the
713 coastal North Sea. Limnology and Oceanography, 56, 2308–2318.
714 Prahl, F.G., Dymond, J., Sparrow, M.A., 2000. Annual biomarker record for export

715 production in the central Arabian Sea. Deep-Sea Research II 47, 1581–1604.
716 Reynolds, R.W., Rayner, N.A., Smith, T.M., Stokes, D.C., Wang, W., 2002. An
717 improved in situ and satellite SST analysis for climate. Journal of Climate 15,
718 1609–1625.
719 Schouten, S., Hopmans, E.C., Pancost, R.D., Sinninghe Damsté, J.S., 2000. Widespread
720 occurrence of structurally diverse tetraether membrane lipids: Evidence for the
721 ubiquitous presence of low-temperature relatives of hyperthermophiles. Proceedings of
722 the National Academy of Science, USA 97, 14421–14426.
723 Schouten, S., Hopmans, E.C., Schefuß, E., Sinninghe Damsté, J.S., 2002. Distributional
724 variations in marine crenarchaeotal membrane lipids: a new tool for reconstructing
725 ancient sea water temperatures? Earth and Planetary Science Letters 204, 265–274.
726 Schouten, S, Huguet, C., Hopmans, E.C., Kienhuis, M.V.M., Sinninghe Damsté, J.S.,
727 2007. Analytical methodology for TEX_{86} paleothermometry by high performance
728 liquid chromatography/atmospheric pressure chemical ionization-mass spectrometry.
729 Analytical Chemistry 79, 2940–2944.
730 Shintani, T., Yamamoto, M., Chen, M.-T., 2011. Paleoenvironmental changes in the
731 northern South China Sea over the past 28,000 years: a study of TEX_{86}-derived sea
732 surface temperatures and terrestrial biomarkers. Journal of the Asian Earth Science
733 40, 1221–1229.
734 Sinninghe Damsté, J.S., Rijpstra, W.I.C., Reichart, G.J., 2002a. The influence of oxic
735 degradation on the sedimentary biomarker record II. Evidence from Arabian Sea
736 sediments. Geochemica et Cosmochimica Acta 66, 2737–2754.
737 Sinninghe Damsté, J.S., Schouten, S., Hopmans, E.C., van Duin, A.C.T., Geenevasen,
738 J.A.J., 2002b. Crenarchaeol: the characteristic core glycerol dibiphytanyl glycerol

739 tetraether membrane lipid of cosmopolitan pelagic crenarchaeota. Journal of Lipid
740 Research 43, 1641–1651.
741 Small, L.F., Fowler, S.W., Ünlü, M.Y., 1979. Sinking rates of natural copepod fecal
742 pellets. Marine Biology 51, 233–241.
743 Spang, A., Hatzenpichler, R., Brochier-Armanet, C., Rattei, T., Tischler, P., Spieck, E.,
744 Streit, W., Stahl, D.A., Wagner, M., Schleper, C., 2010. Distinct gene set in two
745 different lineages of ammonia-oxidizing archaeal supports the phylum
746 Thaumarchaeota. Trends in Microbiology, 18, 331–340.
747 Stuiver, M., Reimer, P., 1993. Extended ^{14}C database and revised CALIB 3.0 ^{14}C age
748 model calibration program. Radiocarbon 35, 215–230.
749 Turich, C., Freeman, K.H., Bruns, M.A., Conte, M., Jones, A.D., Wakeham, S.G., 2007.
750 Lipids of marine Archaea: Patterns and provenance in the water-column and
751 sediments. Geochimica et Cosmochimica Acta, 71, 3272–3291.
752 Verala, M.M., van Aken, H.M., Sintes, E., Herndl, G.J., 2008. Latitudinal trends of
753 Crenarchaeota and Bacteria in the meso- and bathypelagic water masses of the
754 Eastern North Atlantic. Environmental Microbiology, 10, 110–124.
755 Wakeham, S.G., Lee, C., 1993. Production, transport, and alteration of particulate
756 organic matter in the marine water column. In *Organic Geochemistry: Principles and*
757 *Appplications* (edited by Engel, M.H. and Macko, S.A.), pp. 145–169. Plenum Press,
758 New York.
759 Wakeham, S.G., Peterson, M.L., Hedges, J.I., Lee, C., 2002. Lipid biomarker fluxes in
760 the Arabian Sea, with a comparison to the equatorial Pacific Ocean. Dee-Sea
761 Research II, 49, 2265–2301.
762 Wakeham, S.G., Lee, C., Peterson, M.L., Liu, Z., Szlosek, J., Putnam, I.F., Xue, J., 2009.

763 Organic biomarkers in the twilight zone–Time series and settling velocity sediment
764 traps during MedFlux. Deep-Sea Research II, 56, 1437–1453.
765 Wuchter, C., Schouten, S., Wakeham, S.G., Sinninghe Damsté, J.S., 2005. Temporal and
766 spatial variation in tetraether membrane lipids of marine Crenarchaeota in particulate
767 organic matter: Implications for TEX_{86} paleothermometry. Paleoceanography 20,
768 PA3013.
769 Wuchter, C., Abbas, B., Coolen, M.J.L., Herfort, L., van Bleijswijk, J., Timmers, P.,
770 Strous, M., Teira, E., Herndl, G.J., Middelburg, J.J., Schouten, S., Sinninghe Damsté,
771 J.S., 2006a. Archaeal nitrification in the ocean. Proceedings of National Academy of
772 Science, 103, 12317–12322.
773 Wuchter, C., Schouten, S., Wakeham, S.G., Sinninghe Damsté, J.S., 2006b. Archaeal
774 tetraether membrane lipid fluxes in the northeastern Pacific and the Arabian Sea:
775 Implications for TEX_{86} paleothermometry. Paleoceanography 21, PA4208.
776 Yamamoto, M., Shimamoto, A., Fukuhara, T., Naraoka, H., Tanaka, Y., Nishimura, A.,
777 2007. Seasonal and depth variations in molecular and isotopic alkenone composition
778 of sinking particles from the western North Pacific. Deep-Sea Research Part I 54,
779 1571–1592.
780 Yamamoto, M., Polyak, L., 2009. Changes in terrestrial organic matter input to the
781 Mendeleev Ridge, western Arctic Ocean, during the Late Quaternary. Global and
782 Planetary Change, 68, 30–37.
783 Zhang, Y., Sintes, E., Chen, J., Zhnag, Y., Dai, M., Jiao, N., Herndl, G.J., 2009. Role of
784 mesoscale cyclonic eddies in the distribution and activity of Archaea and Bacteria in
785 the South China Sea. Aquatic Microbial Ecology 56, 65–79.
786

787 Table Captions:

788

789 Table 1 Location, sampling periods and trap depths of the WCT-2 mooring sediment
790 trap system

791

792 Table 2 Averaged sinking fluxes of glycerol dialkyl glycerol tetraethers (GDGTs) and
793 flux-weighted TEX_{86}^{H}- and TEX_{86}^{L}-based temperatures (FWT-H and FWT-L) at
794 site WCT-2.

795

796 Table 3 Half-depths and the estimated fluxes at the sea surface (F_0) and sea floor (F_{5389})
797 of GDGTs at site WCT-2.

798

799 Table 1

Location	Seafloor depth (m)	Duration	Trap depth (m)		
			Shallow	Middle	Deep
39□00.09'N, 146□59.66'E	5356	19 November 1997 to 6 August 1998	1366	3056	4786
39□01.00'N, 147□00.06'E	5322	27 August 1998 to 10 August 1999	1332	2472	4752

800

801

802 Table 2

Sampling interval	Duration	Trap position	Depth (m)	GDGT μg m^{-2} d^{-1}	FWT-H (°C)	FWT-L (°C)
NH97	19 Nov 1997 to 6 Aug 1998	Shallow	1366	12.6	13.5	15.4
	19 Nov 1997 to 10 Aug 1998	Middle	3056	6.8	13.8	16.2
	19 Nov 1997 to 6 Aug 1998	Deep	4786	6.2	13.7	15.6
NH98	27 Aug 1998 to 10 Aug 1999	Shallow	1332	16.4	14.2	16.2
	27 Aug 1998 to 10 Aug 1999	Middle	2472	14.2	14.0	16.3
	27 Aug 1998 to 10 Aug 1999	Deep	4752	7.8	13.5	15.4

FWT-H = flux-weighted TEX_{86}^{H}-based temperature.

FWT-L = flux-weighted TEX_{86}^{L}-based temperature.

803

804 Table 3

	Unit	NH97	NH98
$Z_{1/2}$	m	3349	3108
F_0	μg m^{-2} d^{-1}	15.28	22.11
F_{5389}	μg m^{-2} d^{-1}	5.01	6.65

805

806 Figure Captions:

807

808 Fig. 1 Map showing the location of the study site (WCT-2).

809

810 Fig. 2 (a) Monthly mean temperatures at various depths. (b) The depth profiles of
811 temperature in different seasons at the WCT-2 site (39°N, 147°E). Data from Conkright
812 et al. (2002). MAM = March to May, JJA = June to August, SON = September to
813 November, DFJ = December to January.

814

815 Fig. 3 Changes in (a) the concentration and (b) sinking flux of GDGTs, (c and d) TEX_{86}^{H}
816 - and TEX_{86}^{L}-based temperatures, and (e) the ratio of caldarchaeol to crenarchaeol from
817 November 1997 to August 1999. The IGOSS weekly SSTs at 39°N, 147°E are from
818 Reynolds et al. (2002).

819

820 Fig. 4 GDGT concentrations and accumulation rates and TEX_{86}^{H}- and TEX_{86}^{L}-based
821 temperatures in core CMC18. Arrows indicate the calendar ages converted from the
822 AMS ^{14}C ages of bulk organic matter.

823

824 Fig. 5 Changes in (a) measured and satellite-based surface chlorophyll-a concentrations
825 and estimated net primary production, the sinking fluxes of (b) $CaCO_3$, opal, organic
826 carbon, and lithogenic material and (c) GDGTs and alkenones, and (d) TEX_{86}^{H}-, TEX_{86}^{L}
827 - and $U_{37}^{K'}$-based temperatures in the shallow trap from November 1997 to August 1999
828 at site WCT-2. Data for measured chlorophyll-a concentrations at 0–50 m depth

(average) and 50–100 m depth (average) at nearby site (39°N, 146.75°E) are from the Fishery Research Agency of Japan (2012). Data for $CaCO_3$, opal, organic carbon and lithogenic material are from Mohiuddin et al. (2002), and data for alkenones and $U^{K'}_{37}$ are from Yamamoto et al. (2007).

Fig. 6 Sinking fluxes of GDGTs at different depths in the water column.

Fig. 7 Depth profiles in the measured temperature and chlorophyll a concentration (Chl-a) when the trap was recovered on 26 August 1998. The TEX^{H}_{86}- and TEX^{L}_{86}-based temperatures of the cup from 24 July to 6 August 1998 and the expected production depths (EPD) are also presented.

Fig. 8 Flux-weighted TEX^{H}_{86}- and TEX^{L}_{86}-based temperatures and mean annual temperature at different depths in the water column. Data for mean annual temperature are from Conkright et al. (2002).

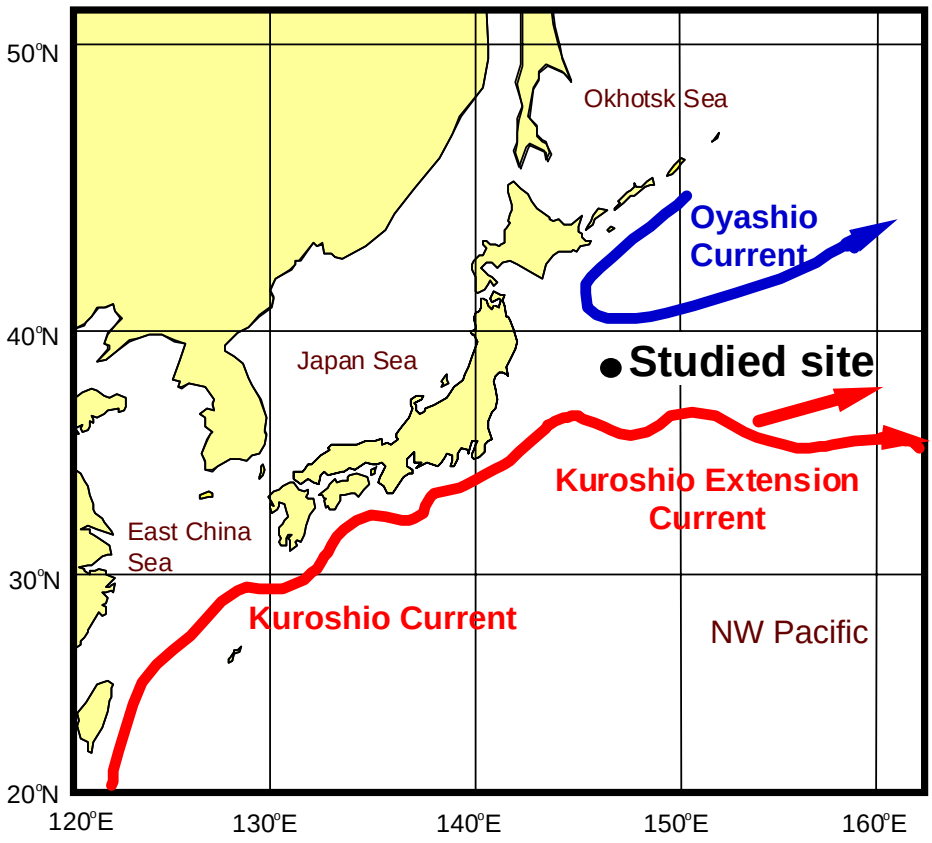

846

847

848 Fig. 1

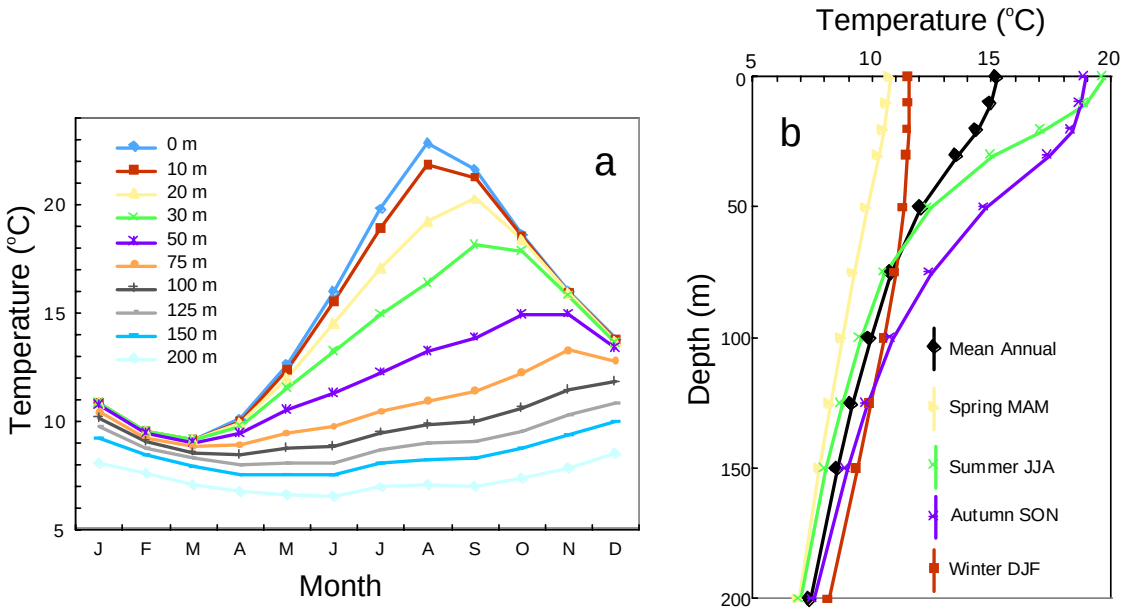

849

850

851 Fig. 2

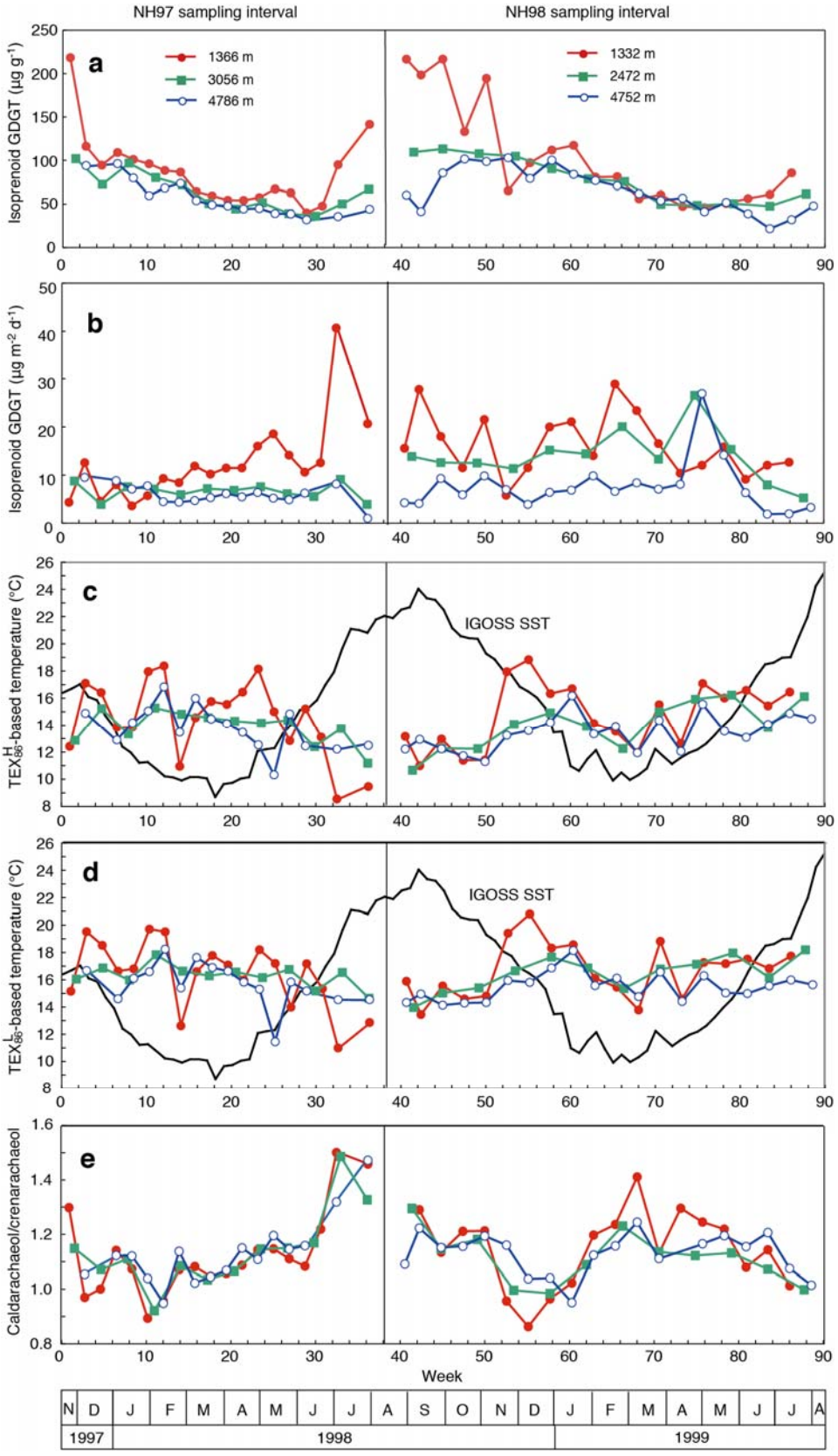
NH97 sampling interval
NH98 sampling interval
a
1366 m
3056 m
4786 m
1332 m
2472 m
4752 m
Isoprenoid GDGT (µg g-1)
b
Isoprenoid GDGT (µg m-2 d-1)
c
IGOSS SST
TEXH86-based temperature (°C)
d
IGOSS SST
TEXL86-based temperature (°C)
e
Caldarachaeol/crenarachaeol
Week
N D J F M A M J J A S O N D J F M A M J J A
1997
1998
1999

852

853 Fig.3

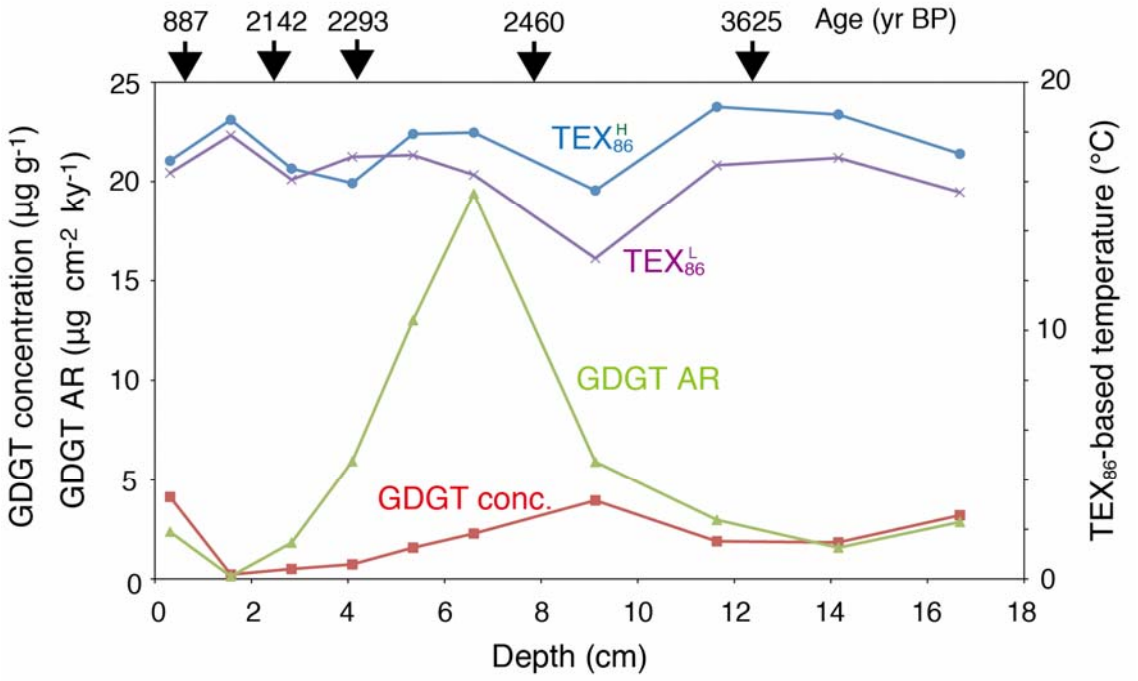
887
2142
2293
2460
3625
Age (yr BP)
TEX$_{86}^{H}$
TEX$_{86}^{L}$
GDGT AR
GDGT conc.
GDGT concentration (µg g^{-1})
GDGT AR (µg cm^{-2} ky^{-1})
TEX$_{86}$-based temperature (°C)
Depth (cm)
0
5
10
15
20
25
0
10
20
0
2
4
6
8
10
12
14
16
18

854

855 Fig. 4

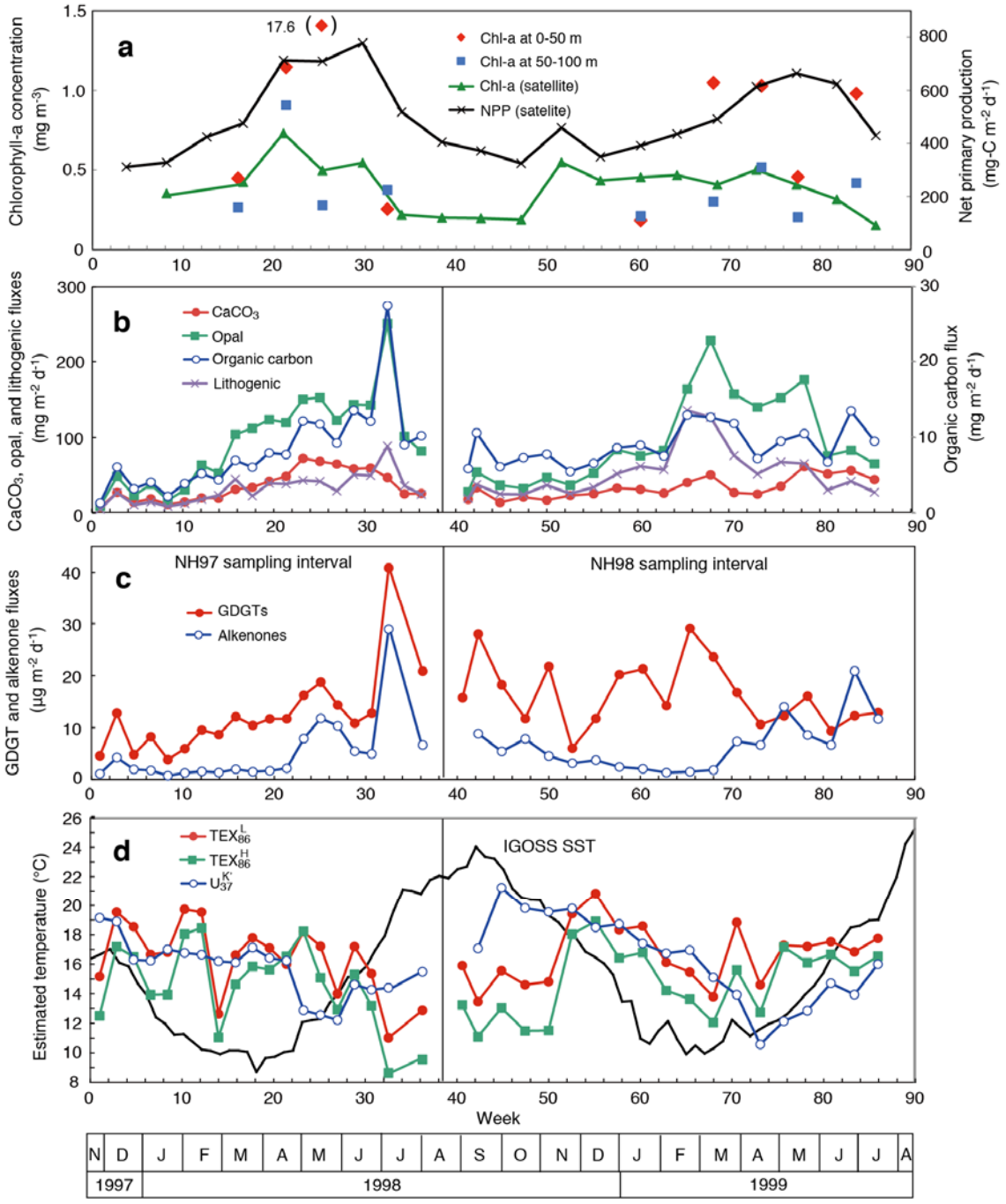
a
17.6
Chl-a at 0-50 m
Chl-a at 50-100 m
Chl-a (satellite)
NPP (satelite)
Chlorophyll-a concentration (mg m-3)
Net primary production (mg-C m-2 d-1)
b
CaCO3
Opal
Organic carbon
Lithogenic
CaCO3, opal, and lithogenic fluxes (mg m-2 d-1)
Organic carbon flux (mg m-2 d-1)
c
NH97 sampling interval
NH98 sampling interval
GDGTs
Alkenones
GDGT and alkenone fluxes (µg m-2 d-1)
d
TEX86L
TEX86H
U37K'
IGOSS SST
Estimated temperature (°C)
Week
N D J F M A M J J A S O N D J F M A M J J A
1997
1998
1999

856

857 Fig. 5

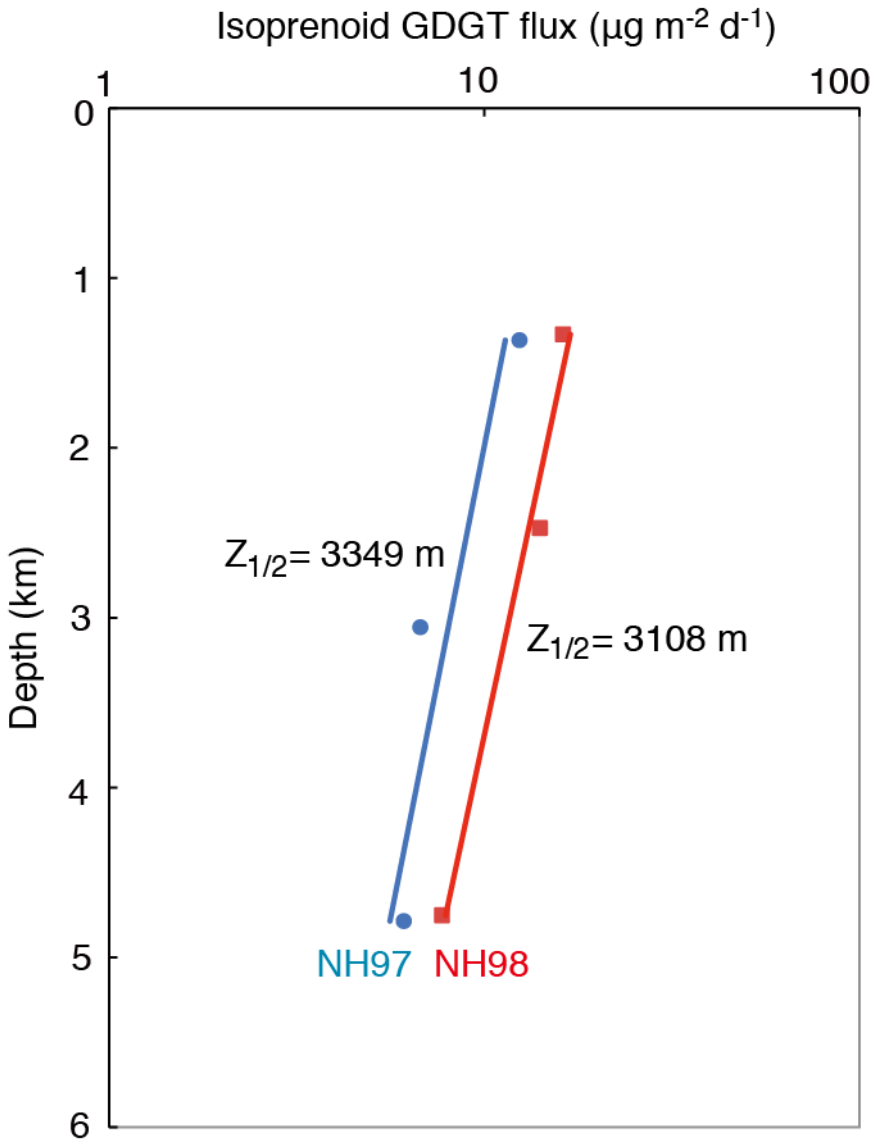

858

859

860 Fig. 6

861

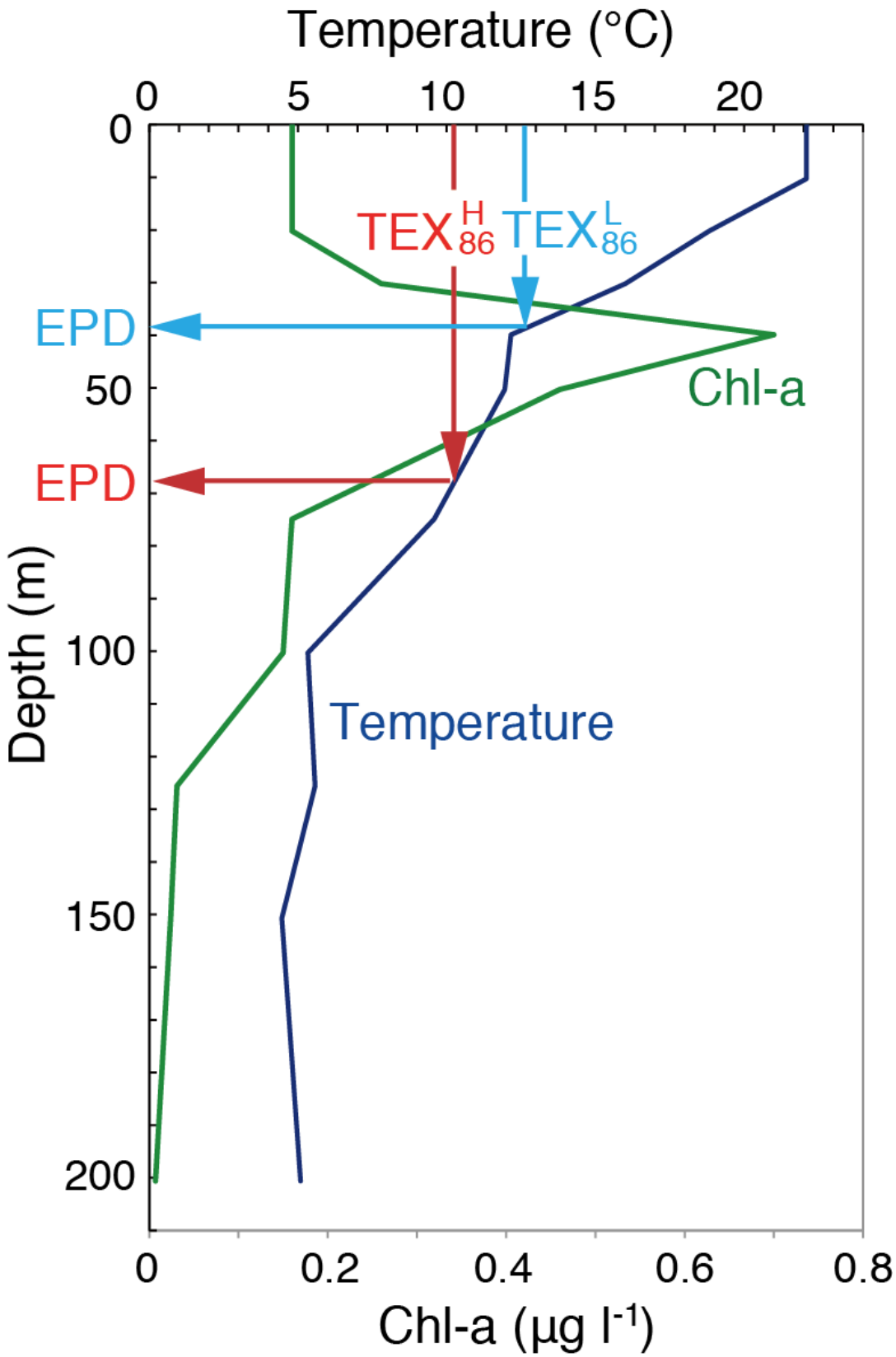
Temperature (°C)
0
5
10
15
20
0
50
100
150
200
Depth (m)
TEX$_{86}^{H}$
TEX$_{86}^{L}$
EPD
EPD
Chl-a
Temperature
0
0.2
0.4
0.6
0.8
Chl-a (µg l^{-1})

862

863 Fig. 7

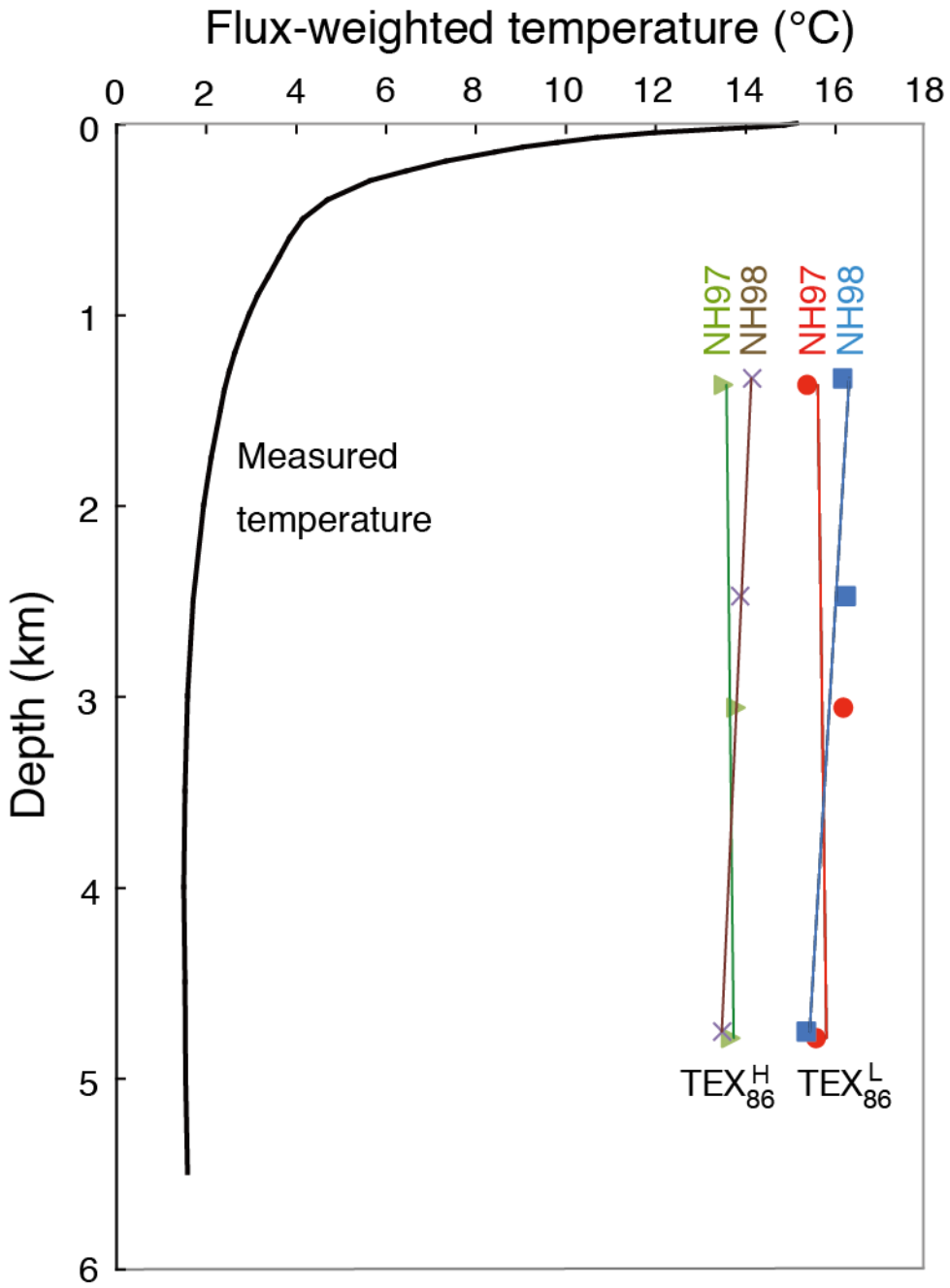
Flux-weighted temperature (°C)
0
2
4
6
8
10
12
14
16
18
Depth (km)
0
1
2
3
4
5
6
Measured
temperature
NH97
NH98
NH97
NH98
TEX$^{H}_{86}$
TEX$^{L}_{86}$

Fig. 8